Wash fastness of Hybrid AlO_x–PET Fabrics Created via Vapor Phase Infiltration

Kira Pyronneau[+•], Emily K. McGuinness[+•], Alan J. Gonzalez[+], Benjamin C. Jean[+], Haley V. Manno[+], Nicole R. McClelland[+], Mark D. Losego[+*]

[+]School of Materials Science and Engineering, Georgia Institute of Technology Atlanta, GA, USA 30332

[•] These authors contributed equally to this work.

*Corresponding author: losego@gatech.edu

Abstract

Vapor phase infiltration (VPI) infuses polymers with metalorganics to create organic-inorganic hybrid materials with properties distinct from the parent polymer. While many studies exist demonstrating the utility of VPI, few studies investigate the stability of the hybrid material's chemical structure and properties under long term use conditions. Herein, the durability to simulated washing is investigated of AlO_x – poly(ethylene terephthalate) hybrid fabrics prepared via VPI with trimethylaluminum (TMA) and water vapor at temperatures of 60, 80, 100, 120, and 140 ˚C under excess TMA infiltration conditions. The inorganic loading of the fabrics varied with temperature with temperatures below 100 ˚C containing ~25 wt% inorganic and fabrics above 100 ˚C having ~17 wt% inorganic as measured by thermogravimetric analysis. Consistent with literature reports, AlO_x – PET fabrics exhibited changes in color and photoluminescence that varied with infiltration temperature. At these high levels of inorganic loading, fabrics infiltrated at lower temperatures (100 ˚C and below) lose a significant quantity of inorganic following washing. This loss is attributed to the formation of highly brittle, oxide-rich hybrid layers that delaminate and are removed during the washing process. At higher infiltration temperatures, negligible inorganic was lost. Decreasing the inorganic loading of fabrics at low infiltration temperatures (by controlling relative precursor / fabric quantity) was found to improve the hybrid fabric's wash durability. In addition to these physical changes, differences in the photoluminescence and chemical structure, indicated by infrared spectroscopy, were observed for all fabrics and provide insights into their chemical structure and degradation pathways.

Keywords: vapor phase infiltration, photoluminescence, inorganic loading, wash fastness, durability

Introduction

Commodity textiles are commonly used as consumer goods such as apparel, carpeting, and upholstery, while technical textiles serve as vital components within a wide range of functional materials from tires to medical stents. Inorganics are often incorporated into polymeric textiles to induce particular properties including flame retardancy[1, 2] and UV-stability.[3, 4] Industrially, liquid-based techniques have been used to add inorganic finishes to textiles. However, laborious soaking and drying steps can be avoided through the use of vapor phase processes.[5, 6] For example, inorganic surface coatings created through atomic layer deposition (ALD, a vapor phase process) on polymer substrates have been shown to create antibacterial textiles,[7, 8] control the wetting behavior of polymer substrates,[9-14] compatibilize the interface of polymer mechanical reinforcements for use in composites,[15, 16] deacidify and provide UV protection to paper,[17] induce electrical conductivity,[6, 18-20] and even transform commodity textiles into flexible resistive heaters.[21] While ALD usually forms an inorganic surface coating, vapor phase processes such as vapor phase infiltration (VPI) can also be used to introduce inorganics into the sub-surface and bulk of a polymer.[22-26] In VPI, a polymer-based material (such as a fabric, fiber, or film) is placed within a reactor where it is exposed to vapor phase metalorganic precursors. Under certain combinations of polymer and precursor chemistry and process conditions, the metalorganic will sorb into the bulk of the polymer material and become entrapped. After the subsequent introduction of an oxidant vapor (e.g., water), the metalorganic reacts within the polymer, forming a metal oxide – polymer hybrid with the same macroscopic form factor as the starting material.[22-28]

VPI has a history of use in transforming fibers and textiles into hybrid materials with enhanced properties. VPI has been used on biopolymer fibers to infiltrate spider dragline silks with titanium dioxide and alumina. The resulting fibers exhibited significant increases in both strength and toughness.[29] Further studies have shown that properties of industrially relevant polymers can be similarly enhanced. VPI modification of textiles specifically has been used to both evoke and preserve new fabric properties.[5, 23-26] Infiltration of polyester fabrics (polyethylene terephthalate [PET] and polybutylene terephthalate) with trimethylaluminum (TMA) and water vapor has created photoluminescent hybrid fabrics[30, 31] for use in photocatalysis,[32] hybrid fibers with enhanced mechanical properties (increased peak load and elongation),[33] and porous monolithic inorganic structures following the removal of the fabric template.[34] Infiltration of Kevlar fibers with diethylzinc (DEZ) and water vapor provided preservation of mechanical properties under UV degradation as well as a general increase in thermal stability.[35] In addition to textile modification, VPI has also been used to stabilize or prepare polymer membranes for use in chemical separations,[28, 36, 37] create hybrid foam oil sorbents,[38] dope electrically conductive polymers,[39-42] and create both nanoscale and macroscale inorganic features from polymer templates.[34, 43-47] Advantages of vapor phase processes such as VPI for modifying textiles includes the absence of

waste-water involved in the VPI process, the ability to perform VPI after the textile has been manufactured into its final form, and the properties available to hybrid materials that cannot be accessed by either the polymer or the inorganic alone. However, the VPI process is still an emerging technology and research is needed to ascertain its feasibility and cost to produce hybrid materials at scale, develop methods for minimizing unwanted property shifts in the creation of the hybrid (for example, increased textile rigidity), and expand both the precursor and polymer chemistries accessible to this technique.

While numerous studies have detailed property enhancements in polymers resulting from VPI, there is a lack of data on how the hybrid materials perform in simulated use environments. Studies on the chemical stability of hybrid materials in organic solvent as well as aqueous environments reveal a dependency on both the chemical structure of the inorganic as well as chemical interactions between the inorganic and polymer.[28, 48] However, no studies exist on the stability of hybrid fabrics prepared via VPI under one of the most common sources of wear on fabrics: washing. During washing fabrics are submerged in water, often at high temperatures, for extended periods of time with agitation. This work investigates the durability to simulated washing of AlO_x – PET fabrics prepared through VPI with trimethylaluminum (TMA) and water vapor created at different temperatures and under two different inorganic loading conditions.

1. Experimental Methods

1.1 Preparation of AlO_x - PET fabrics: Neat PET fabrics were obtained from TestFabrics (Spun Polyester Type 54, Disperse Dyeable). Fabrics were used as received. Infiltration of the fabrics was performed in a custom-built reactor using the precursor trimethylaluminum (room temperature, Strem Chemicals, 98%, **DANGER: pyrophoric**) and co-reactant deionized water vapor dosed from a container at room temperature. Fabrics were infiltrated under two conditions, one termed “maximally infiltrated” or “excess TMA” where excess TMA (estimated via the ideal gas law from pressure dosed into an empty chamber) was provided with respect to the quantity of carbonyl groups present (estimated from fabric mass). The maximally infiltrated results are presented in sections 2.1 and 2.2 of this work. The other condition for infiltration was under “excess polymer” or “limiting TMA reactant” conditions where an insufficient quantity of precursor was introduced to fully saturate the carbonyl groups present. These partially infiltrated fabrics are explored in section 2.3 of this work. The fabrics were placed within the heated reactor and pumped down to rough vacuum with a rotary vane vacuum pump (approximately 30 mTorr, pressures measured with a Baratron capacitance manometer). Then the chamber was purged with nitrogen at ~1.5 Torr for at least one hour to remove sorbed water. The chamber was then pumped down to base vacuum again, isolated, and the TMA precursor valve was opened briefly (about 3 seconds) to achieve a TMA partial pressure of approximately 800 mTorr in the 1 ft^3 chamber. The fabrics were exposed to the static TMA atmosphere for two hours to allow the precursor to sorb and diffuse into the fibers. The chamber was then purged with 1.5 Torr of

nitrogen for 5 minutes to remove excess TMA from the chamber. The fabrics were then exposed to DI water vapor (~2 to 2.5 Torr depending on room temperature) to co-react with the TMA. Water vapor was held in the isolated chamber for 2 hours. Then the chamber was purged with nitrogen for 5 minutes to remove any byproducts prior to opening the chamber.

Fabrics were infiltrated at the following processing temperatures: 60, 80, 100, 120, and 140 °C. For hybrid fabrics created at infiltration temperatures below 100˚C, the entire chamber was set to this temperature. For hybrid fabrics created at 120 and 140 ˚C, the chamber walls were set to 110 ˚C and a small portion at the bottom of the chamber was set to the higher temperature. Fabrics were placed in this hotter region. Representative pressure profiles for these processes are provided in Figures S1 and S2. All dosing sequences were accomplished with a custom-built control software described previously.[49]

1.2 Scanning Electron Microscopy/ Energy Dispersive X-Ray Analysis (SEM/EDX): Elemental analysis of fabric cross-sections was performed with a Phenom ProX benchtop scanning electron microscope. Cross sections of hybrid fabrics were prepared for analysis by cryo-cutting in liquid nitrogen to avoid deforming the fibers. Images were scanned at 15 keV in backscatter mode. EDX profiles were created using the same instrument.

1.3 Thermogravimetric Analysis (TGA): The inorganic loading and decomposition temperatures of the hybrid fabrics were analyzed using thermogravimetric analysis in air (TGA, PerkinElmer TGA 4000). Small portions of fabrics (8-15 mg) were used. Fabrics heated in ~20 mL / min of flowing air to 120 °C and held at this temperature for 50 minutes to remove water from the fabric. The mass after 50 min at 120 °C is deemed the true mass of the dried fabric. Mass is then measured at a rate of 10 ˚C / min to a temperature at which all organic components are combusted (> 700 ˚C). Inorganic weight percent loading is calculated as the mass of the fabric at the maximum temperature divided by the fabric mass at the end of the drying period.

1.4 Fourier Transform Infrared (FTIR) Spectroscopy: FTIR spectra were obtained using a Shimadzu IR-Prestige 21 spectrometer with a Pike attenuated total reflectance (ATR) attachment (diamond crystal). Each spectrum was measured with 64 scans from 400 to 3500 cm-1 at 4 cm-1 resolution. Prior to each FTIR session, a background scan that consisted of 64 scans without fabrics placed on the instrument was performed.

1.5 Simulated Wash Testing: To simulate extreme and repeated washing or environmental degradation, fabrics (approximately 40 mg) were boiled in deionized water (approximately 150 mL, VWR, ASTM II) within a round-bottom flask with a condenser to reclaim vaporized water. A stir bar was used to provide agitation. Detergent was not used for data reported in Sections 2.2 and 2.3. Approximately 0.5 mL of Tide Original laundry detergent was added for the data reported in Section 2.4 The boiling tests were carried out at 100 °C for 90 minutes. Fabrics were

then allowed to dry in ambient conditions (room temperature and humidity) at least overnight prior to further characterization.

1.6 UV-Vis Spectroscopy: UV-Vis spectra were collected using an Avantes Starline AvaSpec 2048 detector and an integrating sphere with a built-in halogen light source. Measurements were taken with the fabric of interest on top of a white reference tile provided by Avantes. Prior to measurement, a dark spectrum was taken with a neat PET fabric placed on the tile and the light source turned off to get an accurate measurement of stray light. The light source was allowed to warm up for 15 minutes and a reference spectrum was taken using the white tile alone. Fabrics were then measured within the same session.

1.7 Photographs: Photographs were taken with a Canon EOS Rebel T5i digital camera with a EFS 18-35 mm lens and image stabilizer under ambient light and a UV Lamp using an F-stop value of 5.6 for both conditions, a shutter-speed of 1/40 for UV and 1/15 for ambient, an ISO of 400 for UV and 800 for ambient, and a white balance setting of "cloudy" for UV and "white fluorescent" for ambient.

2. Results and Discussion

2.1 Physical Characterization of Maximally Vapor Phase Infiltrated AlO_x – PET Fabrics as a Function of Temperature

The AlO_x-PET system has been chosen for this work for two reasons: (1) the ubiquity of PET as a commodity textile and (2) the large number of prior studies into the infiltration of PET with TMA that represent its interest in the VPI field.[30-34, 50-52] Prior reports have established that VPI of PET materials with TMA and water vapor results in hybrid materials with a large quantity of inorganic[33, 52] and intriguing changes in both color and photoluminescence.[30-32] These hybrid materials have been further demonstrated to have applications in areas such as photocatalysis[32] and photoluminescent patterning.[31]

In this study, AlO_x – PET hybrid fabrics are created at infiltration temperatures of 60, 80, 100, 120, and 140 ˚C. Fabrics are infiltrated following a nitrogen purging step to remove residual water from the chamber and fabrics. The chamber is then evacuated to rough vacuum and isolated before the introduction of trimethylaluminum. This precursor exposure step is conducted for two hours based on *in situ* quartz crystal microbalance time to saturation curves in literature.[33] The chamber is then purged for five minutes to remove excess precursor from the reactor environment before a two hour water vapor exposure step to create the final metal oxide hybrid. This process is shown via chamber pressure vs. process time plots for each experiment in **Figure S1**. For the initial portion of this work, a sufficient quantity of TMA is provided within the reactor to be in excess of the carbonyl functional groups (known to interact with TMA) of the fabric within. Conditions where the TMA is a limiting reactant are presented in Section 2.3 of this work.

Throughout this work these will be referred to as excess TMA (or “maximal loading”) and excess polymer (“limiting reactant”) conditions respectively.

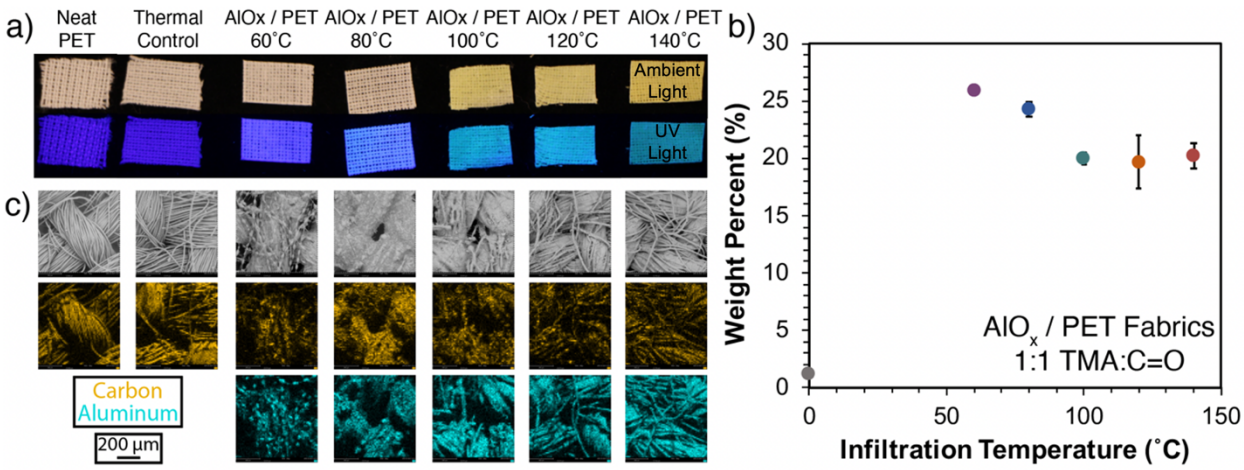

Figure 1. Physical characterization of neat, thermal control, and AlOx / PET fabrics infiltrated with a 1:1 TMA:C=O ratio at 60, 80, 100, 120, and 140 ˚C. a) Physical appearance under ambient and UV light b) inorganic loading as measured by TGA for the fabrics as a function of infiltration temperature with error bars representing the standard deviation of three TGA measurements taken from different locations on a single fabric and c) plane-view SEM images with EDX mapping showing carbon and aluminum signals.

Consistent with the literature reports, excess TMA infiltrated PET fabrics exhibit visual color changes in both ambient and UV light.[30-32] **Figure 1a** shows that in ambient light, fabrics treated at 80 °C and below appear unchanged from the untreated control fabric. However, fabrics treated at 100 ˚C and above have a yellow color that increases in intensity with further increases in infiltration temperature. To probe the source of this color change and photoluminescence, thermal control fabrics are processed using the same conditions (including temperatures, times, and water dosing) without the TMA dose step (extended hold in a vacuum atmosphere replaced the hold in the TMA atmosphere). These fabrics show no change in color or photoluminescence under even the most extreme conditions (four simulated VPI cycles at 140 ˚C) demonstrating that the color change is not a result of degradation from elevated temperatures in the reactor but rather indicative of a shift in reaction between TMA and PET at these higher temperatures (**Figure 1a**). When observed under UV light, the infiltrated fabrics also exhibit a significant increase in photoluminescence as compared to the untreated control with a similar temperature dependency. These shifts are quantified via UV-Vis measurements (*vide infra*) and the chemical mechanisms likely responsible for these optical properties will be presented later in this work.

The weight percent loading of inorganic as measured by thermogravimetric analysis (TGA, calculated as described in the experimental section) at each infiltration temperature is shown in **Figure 1c.** All fabrics show a significant quantity of inorganic (19-26 wt% inorganic). As a result of the large quantities of inorganic within these fabrics, hybrid fabrics created at all temperatures increase dramatically in rigidity following infiltration, as would be expected for a ceramic-loaded material. These mechanical property shifts are consistent with observations made by Padbury and Jur where high quantities of AlO_x infiltrated into PET fibers at 50 ˚C are found to decrease

elongation and peak load to varying extents depending upon initial fiber crystallinity.[33] As a function of infiltration temperature, the inorganic loading decreases continuously from 60 to 100 ˚C and then remains fairly constant from 100 to 140 ˚C. These results match literature reports that found a similar trend for inorganic loading as a function of temperature for the same infiltration system with higher quantities of TMA.[30] This trend is likely due to a combination of factors, one of which may be the known change in reaction mechanism for carbonyl containing polymers around 110 ˚C.[30, 32, 34, 48, 53-57] Another mechanism for this difference in inorganic loading may be variations in the formation of an impermeable hybrid layer in these fabrics. Impermeable layers form in VPI when the hybrid material's structure slows and ultimately stops the diffusion of further precursor into the polymer. At higher temperatures, reactions are likely to occur at a faster rate leading to an earlier formation of the impermeable layer and equating to lower quantities of inorganic loading. Impermeable layers in hybrid materials created via VPI reflect the competition between diffusion and reactions. Resultant hybrid materials that more hinder diffusion kinetics will more significantly limit infiltration.[30, 58, 59]

To understand how infiltration temperature influences the physical structure of the hybrid fabrics, further characterization was performed via SEM and optical microscopy. **Figure 1c** shows plane-view SEM images accompanied by EDX elemental maps for carbon and aluminum for neat PET, thermal control PET, and AlO_x / PET hybrid fabrics. As expected, the PET fibers are largely unchanged by the thermal control process. Upon infiltration at 60 ˚C, fibers in close proximity merge together forming a "monolithic yarn" while fibers not immediately adjacent to others form a "beads on a chain" morphology. In the EDX maps shown in **Figure 1c** and **Figure 2** higher resolution maps reveal striations of carbon rich and aluminum rich regions along the length of the underlying yarn. The presence of carbon rich and aluminum poor regions indicates incomplete infiltration of the fibers. However, the width of carbon rich striations are smaller than the width of the original fibers making it unlikely that these structures form due to surface coatings of the fibers. These observations support the hypothesis of an impermeable layer forming during infiltration. These yarns further show a multitude of cracks indicating their brittle (ceramic-like) nature. The "beads on a chain" single fibers contain "beads" that are greater in thickness than the original fibers and "chains" that are thinner, perhaps representing a mechanism driven by localized heating and surface area minimization.

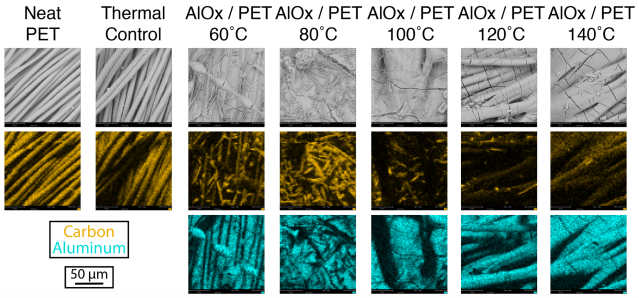

Figure 2. Higher magnification top-view SEM images and EDX maps of neat, thermal control, and AlOx / PET fabrics infiltrated with excess TMA:C=O ratio at 60, 80, 100, 120, and 140 ˚C.

Increasing VPI temperature to 80 ˚C, the "beads on a chain" features are largely removed and a highly brittle, hybrid yarn results. Additionally, yarns intersecting at points of the woven structure seem to fully merge together. Similar to the 60 ˚C infiltration, numerous cracks appear on the surface of these monolithic yarns. While regions that are aluminum rich and carbon rich still appear in the EDX map, the striations observed at the lower temperatures are no longer apparent and rather exist as shorter segments at random orientations.

At 100 ˚C, single fibers begin to re-emerge, but fibers are still highly connected with each other and significant cracks in the material are present. EDX maps show significantly less variation within the hybrid materials structure. Fabrics infiltrated at 120 and 140 ˚C appear similar in SEM image with a number of distinct fibers still with multiple points of interconnection and cracks. In the EDX maps, these materials exhibit little to no regional discrepancies in elemental signal. Optical microscopy corroborates the structures observed in SEM (**Figure S3**).

While the presence of cracks and some fusion of fibers have been reported previously for the infiltration of TMA into PET,[30] the observation of the "beads on a chain" morphology and the highly brittle, ceramic-like fibers has not been previously reported. To verify that the trends observed with temperature represent the infiltration system and not the influence of residual water in the fabrics (especially at low temperatures), an experiment was run where the fabric was first purged in the reactor at 140 ˚C for 6 hours before running the VPI process at 80 ˚C (without breaking vacuum). The results of this study are presented in **Figure S4** and show similarities in inorganic loading, physical appearance, and top-view morphology to the fabrics processed with the standard recipe.

Overall, the hybrid fabrics before washing show temperature dependency in inorganic loading, color and photoluminescence, and physical structure with the likely formation of an impermeable hybrid layer for each temperature under these conditions.

2.2 Wash fastness of Inorganic Loading, Physical Properties, and Chemical Structure for Maximally Infiltrated AlO_x – PET Fabrics

To explore how these differences in physical and chemical structure influence wash fastness, maximally infiltrated hybrid fabrics were boiled in ASTM Type II water for 90 minutes with a stir bar added for agitation. **Figure 3a** presents the inorganic loading (measured via TGA in air) for thermal control and maximally infiltrated hybrid fabrics before and after boiling. As expected, thermal control fabrics show no differences in mass remaining after thermo-oxidative degradation. Hybrid AlO_x / PET fabrics prepared at 60 and 80 °C exhibit significant mass loss upon simulated washing (> 9 wt%), 100 °C exhibits modest mass loss (~3 wt%), and 120 and 140 ˚C hybrid fabric exhibit effectively no mass loss within the measurable error of this TGA method.

SEM / EDX characterization (**Figure 3c**) reveals a likely mechanism for this loss in inorganic loading. At low infiltration temperatures (60-100 ˚C) where inorganic loss was observed, a large quantity of hybrid material is delaminated from the underlying fiber and removed. Higher infiltration temperatures preserve the majority of their hybrid layers with minimal delamination.

However, a significant reduction in carbon signal from the hybrid material is observed possibly indicating a change in chemical state of the hybrid fabric. This temperature dependent result is consistent with previous chemical stability work where AlO_x – PMMA hybrid thin films created at low infiltration temperatures demonstrated poor aqueous stability via a loss of the inorganic while hybrid thin films created at higher infiltration temperatures demonstrated robust stability. This result suggests that the inorganic created at low infiltration temperatures is more susceptible to damage by water.[48] Additionally, high temperature infiltration has demonstrated utility for increasing the adhesion of metal films to polymers shifting the failure mechanism during peel testing away from failure at the interface of the metal and polymer to failure within the polymer bulk, possibly at the point where the hybrid organic-inorganic layer ends.[60]

In terms of macroscale appearance, few changes in color and structure are observable under ambient light as shown in the photographs of **Figure 3b**. However, under UV illumination, clear color changes are observed. To quantify these shifts optical properties, UV-Vis was performed on the control and hybrid fabrics before and after washing (**Figure 4a and b**). UV-Vis absorption spectra of the neat and hybrid fabrics before washing mirror literature results.[30] In both literature and this work, greater and broader absorption is observed for fabrics infiltrated at higher temperatures (consistent with their yellow appearance) while smaller absorption primarily in the UV is observed for fabrics infiltrated at low temperatures. Following washing, the hybrid fabrics prepared at 60 and 80 ˚C that demonstrate a loss in inorganic similarly show a large decrease in UV absorption. Interestingly, the hybrid fabrics infiltrated at 100 ˚C and 120 ˚C demonstrate a slight increase in absorption despite contrary trends in inorganic loading following washing while the fabric infiltrated at 140 ˚C exhibits a decrease in absorption. These differences may be indicative of subtle shifts in the chemical structure of the hybrid materials.

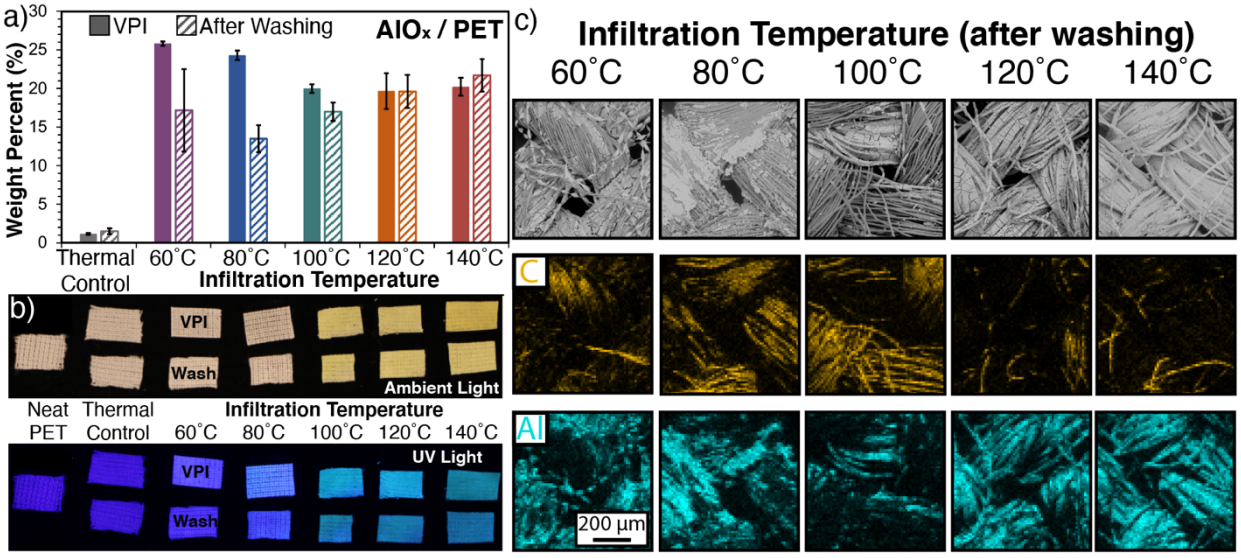

Figure 3. Characterization of thermal control and maximally infiltrated (>1:1 TMA to C=O) hybrid AlOx / PET fabrics before (VPI) and after washing (After Washing) at 100 ˚C in boiling water with agitation for 90 minutes a) inorganic loading as quantified by TGA with error bars representing the standard deviation of

three TGA's taken from different locations on the fabrics (after VPI alone is represented by solid bars while after VPI and washing is represented by striped bars) b) physical appearance under ambient and UV light and c) SEM images and EDX maps after washing with aluminum and carbon signal highlighted.

To determine if shifts in chemical structure were responsible for the observed variations in photoluminescence both as a function of temperature and as a function of simulated washing, FTIR spectra are obtained for all hybrid fabrics before and after washing (**Figure 4c**). A peak table presented in **Table 1** along with difference spectra in **Figure S5** also showcase the changes in peak locations and intensities.

Changes in chemical structure as a function of temperature for hybrid AlO_x / PET fabrics has been explored previously with both FTIR and XPS for fabrics infiltrated with varying quantities of TMA.[30, 32] In the lower wavenumber region, absorptions relevant to PET are overall seen to decrease following infiltration, likely due to the large quantity of inorganic overwhelming the organic signal. For all fabrics the carbonyl peak at 1710 cm^{-1} is greatly decreased with near complete removal observed at 80, 100, and 140 ˚C. New absorptions at 1598 and 1525 cm^{-1} are detected in this work for hybrid fabrics infiltrated under excess TMA conditions at 100, 120, and 140 ˚C. The appearance of these absorptions only at higher infiltration temperatures indicates new reactions and new bond formation at these higher infiltration temperatures.

This observation is consistent with several prior reports of temperature dependent reactions for the TMA + H_2O infiltration of polymers containing ester groups. In the investigations into the photoluminescence of hybrid AlO_x - PET fabrics, in literature two new FTIR absorptions appearing in this region have been observed for fabrics infiltrated at 120 and 150 ˚C. At lower infiltration temperatures of 60 and 90 ˚C these absorptions did not appear.[30] Similarly, in the infiltration of poly(butylene terephthalate) with TMA and water at 80˚C the appearance of absorptions in this region was not observed.[34] These results parallel those observed for the infiltration of poly(methyl methacrylate) [another ester containing polymer] with TMA and water. The TMA / PMMA system exhibits a shift in reaction mechanism near 110 ˚C where infiltration below this temperature does not result in new IR absorptions in this region and infiltration above this temperature results in the appearance of an absorption around 1568 cm^{-1}.[48, 53-57] Interestingly, the infiltration of PMMA at high temperatures also results in a hybrid material with a yellow color, possibly pointing to similarities in ultimate hybrid material structure.[48, 57]

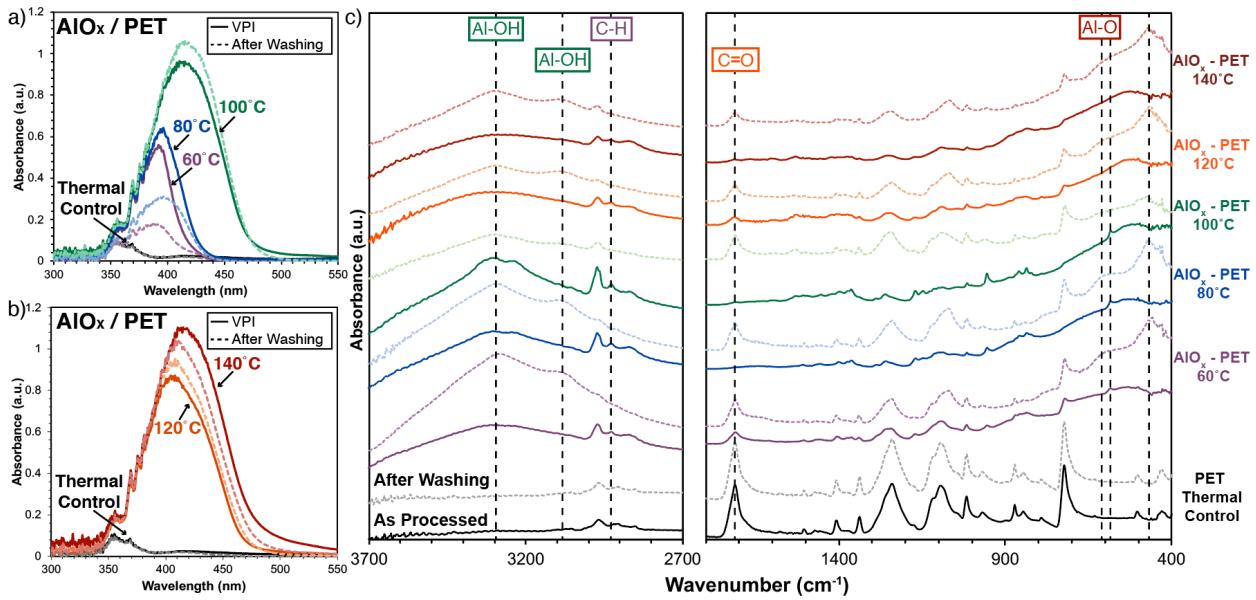

Figure 4. UV-Vis spectra for thermal control PET and PET fabrics maximally infiltrated with TMA (1:1 TMA to carbonyl) at a) 60-100 ˚C and b) 120-140 ˚C before and after simulated washing at 100 ˚C for 90 minutes with agitation. c) FTIR spectra of control PET and PET fabrics maximally infiltrated with TMA (1:1 TMA to carbonyl) before and after simulated washing.

While the temperature dependent change in reaction mechanism is agreed upon in literature, the exact structure of the hybrid material is still an area of active study. Most literature agrees that at low infiltration temperatures, a metastable association between TMA and the ester group of the polymer forms. Upon the introduction of water, this state reverses and the inorganic is unbound from the polymer.[30, 32, 34, 48, 53-57] At higher infiltration temperatures it is also agreed upon that a covalent bond forms between the polymer and the inorganic; and this organic-inorganic bond remains after the introduction of water as a co-reactant. However, the proposed mechanism and final state of the hybrid material ranges from a pericyclic activation of the ester to form a metal acetate (PMMA/TMA),[53, 54] a methylation reaction where a methyl from TMA shifts to the carbon center (PMMA/TMA),[55, 56] and a chain scission event that results in a quinone-like end product (PET/TMA).[30, 32] To elucidate the true structure of hybrid AlO_x – PET fabrics, a dedicated study of fully infiltrated materials with multiple chemical characterization techniques is likely required and beyond the scope of this current work.

After simulated washing, the carbonyl peak of all hybrid fabrics is regenerated to some extent, although its signal intensity remains lower than that observed in neat PET. This return of the carbonyl stretch suggests a possible change to the chemical interaction between the inorganic and the polymer whereby the strength of the interaction decreases such that this vibration is now stronger. At low process temperature, this increase in the carbonyl stretch may also partially result from the removal of hybrid material exposing the uninfiltrated portion of the PET fiber

below, but this explanation cannot be used for the re-emergence of this carbonyl stretch for hybrid fabrics produced at high process temperatures.

The peak that appears at 1598 cm^{-1} for infiltration at 120 and 140 ˚C disappears upon washing while the peak at 1525 cm^{-1} is maintained. This indicates that the nature of the interaction between the polymer and the inorganic is likely changing, but some association remains. The fairly consistent chemical structure of this bond likely contributes to the consistent visual coloration of the fabrics before and after washing.

Infiltration temperature dependent absorptions also arise at 1140 (80 and 100 ˚C) and 1360 cm^{-1} (60-100 ˚C) for lower infiltration temperatures. The weak absorption at 1140 cm^{-1} is likely indicative of a high abundance of hydroxyl groups at these temperatures.[61] Meanwhile the weak absorption at 1360 cm^{-1} likely reflects a small amount of interaction occurring between the polymer and the inorganic, possibly in the form of a metal carboxylate.[62]

An increase in absorption intensity at 2972 cm^{-1} is also seen for infiltration temperatures below 100 ˚C in this work and 90 ˚C in literature and is likely due to the presence of additional methyl groups.[30] This absorption disappears on washing for hybrid fabrics infiltrated at all temperatures. The additional methyl groups could be due to the presence of unreacted TMA ligands. However, due to the extensive water exposure during the VPI process, we believe this explanation is unlikely. Instead these absorptions are perhaps evidence of small molecule byproducts from PET degradation events resulting from the highly exothermic reaction of TMA with water inside the fabric; these small molecule byproducts could then be removed from the fabric upon washing.

Table 1. *FTIR absorption locations and relative peak intensities/shapes for neat PET and fabrics infiltrated at 60, 80, 100, 120, and 140˚C before and after simulated washing. Gray color indicates an absorption found in neat PET, yellow indicates an absorption that appears on infiltration, and blue shows an absorption that appears in infiltrated fabrics after washing.*

Wavenumber (cm-1)	Description	Neat PET	AlOx / PET 60˚C		AlOx / PET 80˚C		AlOx / PET 100˚C		AlOx / PET 120˚C		AlOx / PET 140˚C	
			VPI	Washed	VPI	Washed	VPI	Washed	VPI	Washed	VPI	Washed
420	Medium											
460	Strong											
503	Medium											
530	Broad											
576	Medium											
595	Broad											
722	Strong											
770	Small, Broad											
791	Small											
837	Broad, Shoulders											
847	Medium											
872	Medium											
896	Small											
952	Medium											
968	Medium											
1015	Strong											
1041	Strong Shoulder											
1068	Medium											
1090	Strong, Slightly Broad											
1118	Shoulder											
1140	Weak											
1173	Weak											
1240	Strong with shoulders											
1260	Strong shoulder											
1339	Strong											
1360	Weak											
1370	Medium, broad											
1407	Strong											
1471	Weak, Broad											
1505	Medium											
1530	Weak, Broad											
1597	Weak, Broad											
1711	Very strong											
2860	Strong											
2920	Strong											
2968	Strong											
3080	Strong, Broad											
3230	Strong, Broad											
3290	Strong, Broad											

Key to Wavenumber Colors	
cm-1	Al-O Absorptions (inorganic)
cm-1	OH Absorptions (inorganic)
cm-1	Absorptions due to interactions between polymer and inorganic

Key to Table Colors	
	Peak found in neat PET
	Peak appears after VPI
	Peak appears after washing

The FTIR spectra for hybrid AlO_x / PET fabrics infiltrated at a range of temperatures also provides information about the structure of the inorganic before and after simulated washing. New absorptions in the lower wavenumber region of the spectra (below 1000 cm^{-1}) can be attributed to the Al-O and Al-OH bonds of the inorganic material (Figure 3, Table 1, color: dark red). At all infiltration temperatures, broad absorptions at 530 and 837 cm^{-1} appear along with an additional narrower absorption at 952 cm^{-1}. Another narrower absorption appears at 576 cm^{-1} for fabrics infiltrated at temperatures 60-100 ˚C. Generally, absorptions appearing at < 900 cm^{-1} are due to

Al-O bonds with exact frequencies depending upon the metal oxide's coordination. In literature, low wavenumber absorptions around 560 and 580 cm^{-1} correspond to octahedrally coordinated aluminum (AlO_6). Absorptions present at 806 and 835 cm^{-1} could be due to either tetrahedrally coordinated aluminum[63, 64] or the presence of aluminum hydroxide.[65] The absorptions at 952 cm^{-1} also suggests the existence of aluminum hydroxide groups;[61, 65, 66] this conclusion is further supported by the hydroxyl stretches at 3290 cm^{-1} found for hybrid fabrics created at all temperatures.[64, 67]

Overall, the presence of these absorptions supports an inorganic structure that is primarily octahedrally (AlO_6) coordinated aluminum that is at least partially hydroxylated. The subtle shifts in these absorptions apparent at different infiltration temperatures is challenging to deconvolute, but likely arise from differences in inorganic structure that merit further chemical characterization.

Upon washing, the absorptions at 530, 576, and 837 cm^{-1} disappear and new absorptions appear for all infiltration temperatures at 460, 595 (broad), 770 (broad), and 1068 cm^{-1}. These differences likely indicate a restructuring of the inorganic, specifically the octahedrally coordinated aluminum. A new absorption at 3080 cm^{-1} may suggest a change in the hydration of this inorganic.

These subtle shifts in the inorganic structure may also explain changes in the photoluminescence and the UV-Vis spectra of these hybrid fabrics beyond the loss of hybrid material from the delamination mechanism. The changes reported here highlight the importance of considering the changes in the inorganic alongside changes in the polymer structure for hybrid materials created via VPI.

2.3 Influence of Washing on Inorganic Loading, Optical Properties, and Chemical Structure for Partially Infiltrated AlO_x – PET Fabrics

In their 2014 work, Akyildiz, Lo, Dillon, Roberts, Everitt, and Jur established that inorganic loading of hybrid AlO_x / PET fabrics can be controlled via the number of TMA doses and that shorter number of doses better preserves the flexibility of the hybrid fabric.[30] We hypothesize that limiting the quantity of TMA available to diffuse into the polymer (via fabric mass and TMA dose pressure) can also control inorganic loading and that less-loaded, more flexible hybrid fabrics could offer improved durability to wash fastness testing. To test this hypothesis and determine if simulated washing durability could be affected by the amount and distribution of inorganic loading, hybrid fabrics were prepared by both increasing the mass of fabric within the reactor and decreasing the TMA dose pressure. These conditions made the VPI process reactant-limited, that is the fabric had more carbonyl binding sites than TMA molecules were available in the reaction chamber. We verified this limited reactant condition by tracking the process pressure, as shown in **Figure 5a.** While chamber pressure only dropped modestly in prior runs (e.g., 2:1

TMA:C=O), the chamber pressure was completely depleted for these limiting reactant conditions (1:25 TMA:C=O).

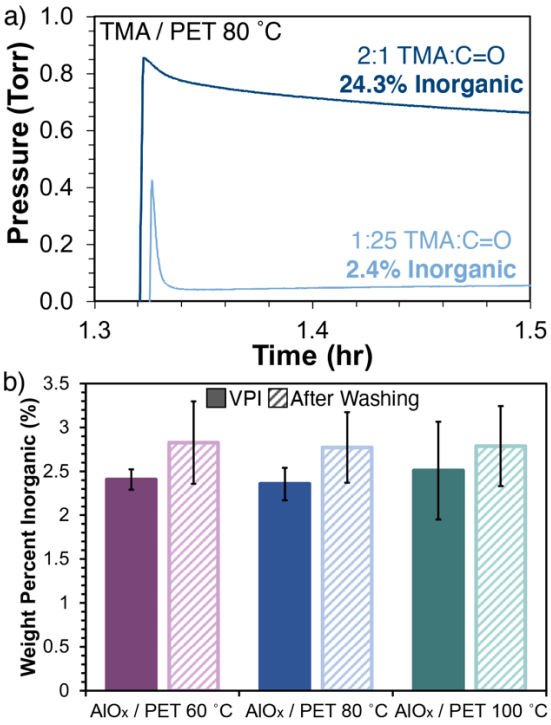

Figure 5. a) *In situ* pressure profiles for the TMA exposure step in the infiltration of PET fabrics for two different molar ratios of TMA to carbonyl functional groups (as controlled by TMA dose pressure and fabric mass). b) Inorganic loading as measured via TGA in air for hybrid AlO_x / PET fabrics created at 60, 80, and 100 ˚C before (VPI) and after washing. Error bars represent the standard deviation of at least three TGA measurements on three replicate hybrid fabrics infiltrated under the same conditions.

Fabrics infiltrated under these excess polymer (limiting reactant) conditions at 60, 80, and 100 ˚C (infiltration temperatures that exhibited poor durability to simulated washing under excess TMA infiltration conditions) were then washed according to the previously described protocol. **Figure 5b** plots the TGA measured inorganic loading before and after simulated washing. The use of excess polymer infiltration conditions (1 TMA to 25 C=O groups) results in an order of magnitude less inorganic loading (2.4 wt% versus 24 wt%) and a more flexible hybrid fabric. To within the accuracy of these TGA measurements, these less loaded hybrid fabrics show no measurable change in inorganic loading after simulated washing. Physical and chemical characterization of these hybrid fabrics along with AlO_x / PET fabrics infiltrated at 120 and 140 ˚C under excess polymer conditions (about 1 TMA to 6 C=O groups) are presented in the supporting information both before and after washing. These characterizations reveal an inorganic that shows physical durability to the boiling water environment, but still undergoes chemical rearrangements similar to the excess TMA infiltrated hybrid fabrics. These results suggest that wash durability can be adjusted with inorganic loading. We propose that this improved durability is attributed to either a less brittle (ceramic-like) hybrid shell or a lower depth of infiltration that improves the adhesion of the hybrid portion to the uninfiltrated fiber below.

2.4 Influence of Detergent on Washing of Hybrid AlO_x – PET Fabrics

Finally, we examined the influence detergent may have on the washing of hybrid AlOx – PET fabrics in boiling water for 90 minutes. Alumina is known to be amphoteric with dissolution behavior observed in both basic and acidic environments.[68] Therefore, detergents may shift the washing environment pH or otherwise influence the hybrid material's stability. To investigate the influence of detergent on washing of hybrid AlO_x – PET fabrics, approximately 0.5 mL of Tide laundry detergent was introduced to the ~150 mL boiling water washing environment. A control PET fabric and representative hybrid fabrics were washed under these conditions including partially infiltrated and maximally infiltrated fabrics infiltrated at 60 and 140 ˚C. The inorganic loading was then quantified once more using TGA as shown in Figure 6a.

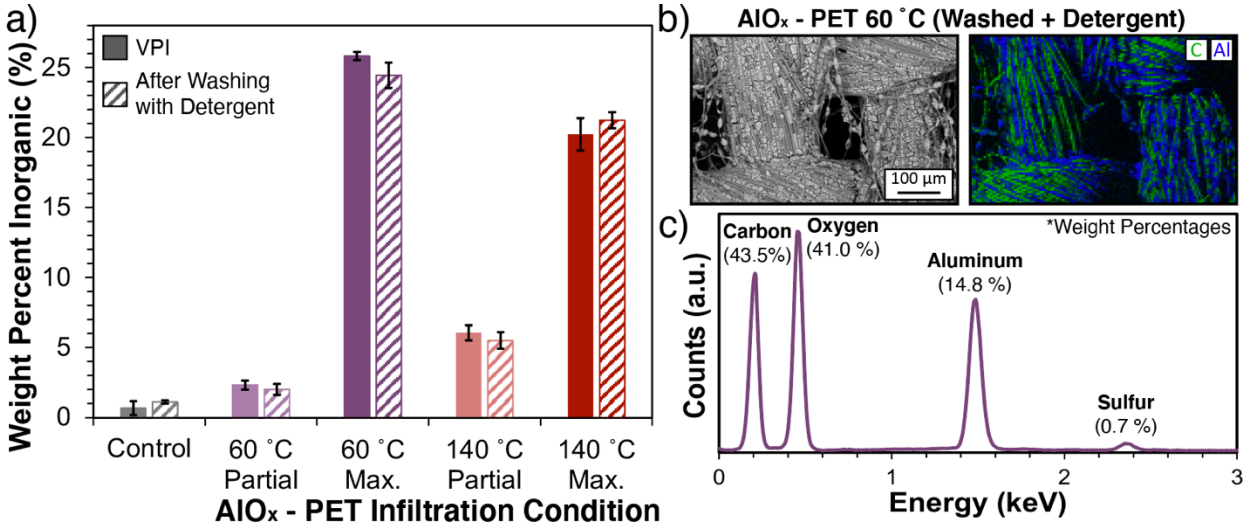

Figure 6. Study of select AlOx – PET fabrics after washing in boiling water with detergent for 90 minutes. a) Inorganic loading as measured by TGA in air of neat PET and AlOx – PET fabrics both partially and maximally infiltrated at 60 and 140 ˚C before and after washing with detergent. Error bars are from three TGA runs of one infiltrated fabric either before or after washing. b) SEM image and EDX map with aluminum and carbon signal highlighted for a maximally infiltrated AlOx – PET fabric created at 60 ˚C after washing with detergent. c) EDX signal counts and weight percent quantification from the map in (b).

Control PET fabrics washed with detergent demonstrated a very slight increase in inorganic loading perhaps pointing to residue on the fabrics that leads to degradation products that remain following washing. Tide laundry detergent contains over eighty chemical components some of which include silicon, aluminum, sodium, sulfur, and chlorine, elements which all may remain following thermal-oxidative combustion of the washed hybrid fabrics (in fact, the presence of sulfur is clearly observed on hybrid fabrics washed with detergent as shown in the elemental signal from EDX mapping in **Figure 5c**). Overall, the trend in results of hybrid fabrics washed with detergent are consistent with those washed with water alone (in boiling water, 90 minutes). Hybrid fabrics created at the low infiltration temperature of 60 ˚C exhibit a loss under maximal infiltration, but stability under partial infiltration while hybrid fabrics created at the high

infiltration temperature of 140 ˚C demonstrate stability both under maximal and partial infiltration. The magnitude of loss for the maximally infiltrated hybrid fabric at 60 ˚C is somewhat less than that under washing in water alone, perhaps pointing to a protective influence of the detergent, but more likely representing variability associated with the washing process. The loss of inorganic for the 60 ˚C maximally infiltrated hybrid AlOx – PET fabric is additionally characterized via SEM imaging and EDX elemental mapping with the resulting image and map presented in **Figure 5b**. Consistent with images from washing with water alone, significant destruction of the hybrid material is observed via a delamination mechanism.

Conclusions

Durability is a critical attribute for the eventual commercial scale-up and application of organic-inorganic hybrid fabrics created via vapor phase infiltration. One frequent source of wear on textile-based materials is the laundering process. This study seeks to understand how aggressive conditions in the form of immersion in boiling water (with and without the addition of detergent) influences the inorganic loading, physical and chemical structure, and optical properties of hybrid fabrics prepared via VPI. In this study, AlO_x / PET fabrics of two different inorganic loading levels are prepared via infiltration with TMA and water vapor at temperatures of 60-140 ˚C. For both inorganic loading levels, the hybrid fabrics exhibit infiltration temperature dependent properties consistent with prior literature reports. At high inorganic loadings (~24 wt%) prepared under excess TMA conditions, hybrid fabrics prepared at temperatures below 100 ˚C lose their fibrous structure and show poor durability to simulated washing via the delamination and loss of the brittle hybrid material. Hybrid fabrics prepared at higher infiltration temperatures demonstrate stability of inorganic loading likely due to their maintenance of a fibrous structure. Decreasing the inorganic loading of hybrid fabrics created at low process temperatures ($\leq$ 100°C) by controlling the quantity of TMA to fabric provided in the reaction chamber is shown to improve wash durability. This result indicates that the durability of the hybrid fabric can be optimized in terms of inorganic loading as well as process temperatures. Additionally, at all temperatures and inorganic loadings, the inorganic undergoes chemical changes as a result of washing that may influence the photoluminescence and other properties of the hybrid fabric. In summary, this work emphasizes how both the chemical (via infiltration temperature) and physical structure (inorganic loading via TMA and fabric quantity) control properties critical to hybrid fabric use and durability.

Supporting Information

Pressure data for all VPI runs; optical microscope characterization; TGA and SEM / EDX characterization of 80 ˚C infiltrated that was first heated at 140 ˚C; hybrid fabric FTIR difference spectra; TGA, FTIR, and SEM / EDX characterization of hybrid fabrics prepared under excess polymer conditions before and afer washing; SEM / EDX of washed control PET fabric

Acknowledgements

K.P., B.C.J., A.J.G., and H.V.M were supported in part by the Georgia Tech President's Undergraduate Research Award (PURA) and the Roxanne D. Westendorf Undergraduate Research Fund. B.C.J. and M.D.L. also received support from the National Science Foundation (DMREF-1921873). E.K.M. was supported by the Department of Defense (DoD) through the National Defense Science & Engineering Graduate (NDSEG) Fellowship Program. Part of this research was conducted in Georgia Tech's Materials Innovation & Learning Laboratory (The MILL), an uncommon ''make and measure'' space committed to elevating undergraduate research in materials science.

Table of Contents Graphic

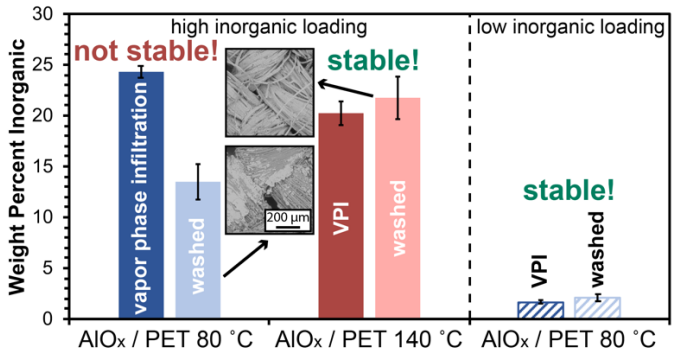

REFERENCES

1. Morgan, A. B.; Gilman, J. W., An overview of flame retardancy of polymeric materials: application, technology, and future directions. *Fire and Materials* **2013,** *37* (4), 259-279.
2. Lopez-Cuesta, J. M.; Laoutid, F., Fire Retardancy of Polymeric Materials. Second ed.; Wilkie, C. A.; Morgan, A. B., Eds. CRC Press - Taylor & Francis Group: Boca Raton, FL, 2010; pp 301-324.
3. Yang, H. Y.; Zhu, S. K.; Pan, N., Studying the mechanisms of titanium dioxide as ultraviolet-blocking additive for films and fabrics by an improved scheme. *Journal of Applied Polymer Science* **2004,** *92* (5), 3201-3210.
4. Broasca, G.; Borcia, G.; Dumitrascu, N.; Vrinceanu, N., Characterization of ZnO coated polyester fabrics for UV protection. *Applied Surface Science* **2013,** *279*, 272-278.
5. Ashurbekova, K.; Ashurbekova, K.; Botta, G.; Yurkevich, O.; Knez, M., Vapor phase processing: a novel approach for fabricating functional hybrid materials. *Nanotechnology* **2020,** *31* (34), 342001.
6. Brozena, A. H.; Oldham, C. J.; Parsons, G. N., Atomic layer deposition on polymer fibers and fabrics for multifunctional and electronic textiles. *J Vac Sci Technol A* **2016,** *34* (1), 10801-10801.
7. Puvvada, R. U.; Wooding, J. P.; Bellavia, M. C.; McGuinness, E. K.; Sulchek, T. A.; Losego, M. D., Bacterial Growth and Death on Cotton Fabrics Conformally Coated with ZnO Thin Films of Varying Thicknesses via Atomic Layer Deposition (ALD). *Jom* **2019,** *71* (1), 178-184.
8. Popescu, M. C.; Ungureanu, C.; Buse, E.; Nastase, F.; Tucureanu, V.; Suchea, M.; Draga, S.; Popescu, M. A., Antibacterial efficiency of cellulose-based fibers covered with ZnO and Al2O3 by Atomic Layer Deposition. *Applied Surface Science* **2019,** *481*, 1287-1298.
9. Lee, K.; Jur, J. S.; Kim, D. H.; Parsons, G. N., Mechanisms for hydrophilic/hydrophobic wetting transitions on cellulose cotton fibers coated using Al2O3 atomic layer deposition. *Journal of Vacuum Science & Technology A: Vacuum, Surfaces, and Films* **2012,** *30* (1), 01A163-01A163.
10. Short, A. E.; Pamidi, S. V.; Bloomberg, Z. E.; Li, Y.; Losego, M. D., Atomic layer deposition (ALD) of subnanometer inorganic layers on natural cotton to enhance oil sorption performance in marine environments. *J. Mater. Res.* **2019,** *34* (4), 563-570.
11. Li, Y.; Chen, L. H.; Wooding, J. P.; Zhang, F. Y.; Lively, R. P.; Ramprasad, R.; Losego, M. D., Controlling wettability, wet strength, and fluid transport selectivity of nanopaper with atomic layer deposited (ALD) sub-nanometer metal oxide coatings. *Nanoscale Advances* **2020,** *2* (1), 356-367.
12. Hyde, G. K.; Scarel, G.; Spagnola, J. C.; Peng, Q.; Lee, K.; Gong, B.; Roberts, K. G.; Roth, K. M.; Hanson, C. A.; Devine, C. K.; Stewart, S. M.; Hojo, D.; Na, J. S.; Jur, J. S.; Parsons, G. N., Atomic layer deposition and abrupt wetting transitions on nonwoven polypropylene and woven cotton fabrics. *Langmuir* **2010,** *26* (4), 2550-8.
13. Gong, B.; Spagnola, J. C.; Parsons, G. N., Hydrophilic mechanical buffer layers and stable hydrophilic finishes on polydimethylsiloxane using combined sequential vapor infiltration and atomic/molecular layer deposition. *J Vac Sci Technol A* **2012,** *30* (1), 01A156-01A156.
14. Waldman, R. Z.; Yang, H. C.; Mandia, D. J.; Nealey, P. F.; Elam, J. W.; Darling, S. B., Janus Membranes via Diffusion-Controlled Atomic Layer Deposition. *Adv. Mater. Interfaces* **2018,** *5* (15), 1800658-1800658.
15. Wooding, J. P.; Li, Y.; Kalaitzidou, K.; Losego, M. D., Engineering the interfacial chemistry and mechanical properties of cellulose-reinforced epoxy composites using atomic layer deposition (ALD). *Cellulose* **2020,** *27* (11), 6275-6285.
16. Chen, Y.; Ginga, N. J.; LePage, W. S.; Kazyak, E.; Gayle, A. J.; Wang, J.; Rodriguez, R. E.; Thouless, M. D.; Dasgupta, N. P., Enhanced Interfacial Toughness of Thermoplastic-Epoxy Interfaces Using ALD Surface Treatments. *ACS Appl Mater Interfaces* **2019,** *11* (46), 43573-43580.
17. Hanson, C. A.; Oldham, C. J.; Parsons, G. N., Paper deacidification and UV protection using ZnO atomic layer deposition. *J Vac Sci Technol A* **2012,** *30* (1), 01A117-01A117.

18. Kalanyan, B.; Oldham, C. J.; Sweet, W. J., 3rd; Parsons, G. N., Highly conductive and flexible nylon-6 nonwoven fiber mats formed using tungsten atomic layer deposition. *ACS Appl Mater Interfaces* **2013,** *5* (11), 5253-9.
19. Jur, J. S.; Sweet, W. J.; Oldham, C. J.; Parsons, G. N., Atomic Layer Deposition of Conductive Coatings on Cotton, Paper, and Synthetic Fibers: Conductivity Analysis and Functional Chemical Sensing Using "All-Fiber" Capacitors. *Adv Funct Mater* **2011,** *21* (11), 1993-2002.
20. Mackus, A. J. M.; Garcia-Alonso, D.; Knoops, H. C. M.; Bol, A. A.; Kessels, W. M. M., Room-Temperature Atomic Layer Deposition of Platinum. *Chem. Mat.* **2013,** *25* (9), 1769-1774.
21. Oh, I. K.; Park, J. S.; Khan, M. R.; Kim, K.; Lee, Z.; Shong, B.; Lee, H. B. R., Reaction Mechanism of Pt Atomic Layer Deposition on Various Textile Surfaces. *Chem. Mat.* **2019,** *31* (21), 8995-9002.
22. Leng, C. Z.; Losego, M. D., Vapor phase infiltration (VPI) for transforming polymers into organic-inorganic hybrid materials: a critical review of current progress and future challenges. *Mater. Horizons* **2017,** *4* (5), 747-771.
23. Waldman, R. Z.; Mandia, D. J.; Yanguas-Gil, A.; Martinson, A. B. F.; Elam, J. W.; Darling, S. B., The chemical physics of sequential infiltration synthesis-A thermodynamic and kinetic perspective. *J Chem Phys* **2019,** *151* (19), 190901.
24. Azpitarte, I.; Knez, M., Vapor phase infiltration: from a bioinspired process to technologic application, a prospective review. *Mrs Communications* **2018,** *8* (3), 727-741.
25. Subramanian, A.; Tiwale, N.; Nam, C.-Y., Review of Recent Advances in Applications of Vapor-Phase Material Infiltration Based on Atomic Layer Deposition. *Jom* **2018,** *71* (1), 185-196.
26. Ingram, W. F.; Jur, J. S., Properties and Applications of Vapor Infiltration into Polymeric Substrates. *Jom* **2018,** *71* (1), 238-245.
27. Leng, C. Z.; Losego, M. D., A physiochemical processing kinetics model for the vapor phase infiltration of polymers: measuring the energetics of precursor-polymer sorption, diffusion, and reaction. *Phys Chem Chem Phys* **2018,** *20* (33), 21506-21514.
28. McGuinness, E. K.; Zhang, F. Y.; Ma, Y.; Lively, R. P.; Losego, M. D., Vapor Phase Infiltration of Metal Oxides into Nanoporous Polymers for Organic Solvent Separation Membranes. *Chem. Mat.* **2019,** *31* (15), 5509-5518.
29. Lee, S. M.; Pippel, E.; Gosele, U.; Dresbach, C.; Qin, Y.; Chandran, C. V.; Brauniger, T.; Hause, G.; Knez, M., Greatly increased toughness of infiltrated spider silk. *Science* **2009,** *324* (5926), 488-92.
30. Akyildiz, H. I.; Lo, M.; Dillon, E.; Roberts, A. T.; Everitt, H. O.; Jur, J. S., Formation of novel photoluminescent hybrid materials by sequential vapor infiltration into polyethylene terephthalate fibers. *J. Mater. Res.* **2014,** *29* (23), 2817-2826.
31. Akyildiz, H. I.; Mousa, M. B. M.; Jur, J. S., Atmospheric pressure synthesis of photoluminescent hybrid materials by sequential organometallic vapor infiltration into polyethylene terephthalate fibers. *J. Appl. Phys.* **2015,** *117* (4), 7.
32. Akyildiz, H. I.; Stano, K. L.; Roberts, A. T.; Everitt, H. O.; Jur, J. S., Photoluminescence Mechanism and Photocatalytic Activity of Organic-Inorganic Hybrid Materials Formed by Sequential Vapor Infiltration. *Langmuir* **2016,** *32* (17), 4289-96.
33. Padbury, R. P.; Jur, J. S., Systematic study of trimethyl aluminum infiltration in polyethylene terephthalate and its effect on the mechanical properties of polyethylene terephthalate fibers. *J Vac Sci Technol A* **2015,** *33* (1), 9.
34. Gong, B.; Peng, Q.; Jur, J. S.; Devine, C. K.; Lee, K.; Parsons, G. N., Sequential Vapor Infiltration of Metal Oxides into Sacrificial Polyester Fibers: Shape Replication and Controlled Porosity of Microporous/Mesoporous Oxide Monoliths. *Chem. Mat.* **2011,** *23* (15), 3476-3485.
35. Azpitarte, I.; Zuzuarregui, A.; Ablat, H.; Ruiz-Rubio, L.; Lopez-Ortega, A.; Elliott, S. D.; Knez, M., Suppressing the Thermal and Ultraviolet Sensitivity of Kevlar by Infiltration and Hybridization with ZnO. *Chem. Mat.* **2017,** *29* (23), 10068-10074.

36. Ogieglo, W.; Puspasari, T.; Hota, M. K.; Wehbe, N.; Alshareef, H. N.; Pinnau, I., Nanohybrid thin-film composite carbon molecular sieve membranes. *Materials Today Nano* **2020,** *9*, 100065-100065.
37. Waldman, R. Z.; Choudhury, D.; Mandia, D. J.; Elam, J. W.; Nealey, P. F.; Martinson, A. B. F.; Darling, S. B., Sequential Infiltration Synthesis of Al2O3 in Polyethersulfone Membranes. *Jom* **2019,** *71* (1), 212-223.
38. Barry, E.; Mane, A. U.; Libera, J. A.; Elam, J. W.; Darling, S. B., Advanced oil sorbents using sequential infiltration synthesis. *J. Mater. Chem. A* **2017,** *5* (6), 2929-2935.
39. Wang, W. K.; Yang, F.; Chen, C. Q.; Zhang, L. B.; Qin, Y.; Knez, M., Tuning the Conductivity of Polyaniline through Doping by Means of Single Precursor Vapor Phase Infiltration. *Adv. Mater. Interfaces* **2017,** *4* (4), 1600806-1600806.
40. Wang, W.; Chen, C.; Tollan, C.; Yang, F.; Beltran, M.; Qin, Y.; Knez, M., Conductive Polymer-Inorganic Hybrid Materials through Synergistic Mutual Doping of the Constituents. *ACS Appl Mater Interfaces* **2017,** *9* (33), 27964-27971.
41. Wang, W.; Chen, C.; Tollan, C.; Yang, F.; Qin, Y.; Knez, M., Efficient and controllable vapor to solid doping of the polythiophene P3HT by low temperature vapor phase infiltration. *J. Mater. Chem. C* **2017,** *5* (10), 2686-2694.
42. Gregory, S. A.; Li, Y.; Monroe, T. D.; Li, J.; Yee, S. K.; Losego, M. D., Vapor Phase Infiltration Doping of the Semiconducting Polymer Poly(aniline) with TiCl4 + H2O: Mechanisms, Reaction Kinetics, and Electrical and Optical Properties. *ACS Applied Polymer Materials* **2021,** *3* (2), 720-729.
43. Kamcev, J.; Germack, D. S.; Nykypanchuk, D.; Grubbs, R. B.; Nam, C. Y.; Black, C. T., Chemically enhancing block copolymers for block-selective synthesis of self-assembled metal oxide nanostructures. *ACS Nano* **2013,** *7* (1), 339-46.
44. Yi, D. H.; Nam, C. Y.; Doerk, G.; Black, C. T.; Grubbs, R. B., Infiltration Synthesis of Diverse Metal Oxide Nanostructures from Epoxidized Diene-Styrene Block Copolymer Templates. *Acs Applied Polymer Materials* **2019,** *1* (4), 672-683.
45. Tiwale, N.; Subramanian, A.; Kisslinger, K.; Lu, M.; Kim, J. Y.; Stein, A.; Nam, C. Y., Advancing next generation nanolithography with infiltration synthesis of hybrid nanocomposite resists. *J. Mater. Chem. C* **2019,** *7* (29), 8803-8812.
46. Berman, D.; Shevchenko, E., Design of functional composite and all-inorganic nanostructured materials via infiltration of polymer templates with inorganic precursors. *J. Mater. Chem. C* **2020,** *8* (31), 10604-10627.
47. Berman, D.; Guha, S.; Lee, B.; Elam, J. W.; Darling, S. B.; Shevchenko, E. V., Sequential Infiltration Synthesis for the Design of Low Refractive Index Surface Coatings with Controllable Thickness. *ACS Nano* **2017,** *11* (3), 2521-2530.
48. McGuinness, E. K.; Leng, C. Z.; Losego, M. D., Increased Chemical Stability of Vapor-Phase Infiltrated AlOx-Poly(methyl methacrylate) Hybrid Materials. *Acs Applied Polymer Materials* **2020,** *2* (3), 1335-1344.
49. Piercy, B. D.; Losego, M. D., Tree-based control software for multilevel sequencing in thin film deposition applications. *Journal of Vacuum Science & Technology B* **2015,** *33* (4), 043201-043201.
50. Gong, B.; Parsons, G. N., Quantitative in situ infrared analysis of reactions between trimethylaluminum and polymers during Al2O3 atomic layer deposition. *J. Mater. Chem.* **2012,** *22* (31), 15672-15682.
51. Akyildiz, H. I.; Jur, J. S., Organometallic exposure dependence on organic-inorganic hybrid material formation in polyethylene terephthalate and polyamide 6 polymer fibers. *J Vac Sci Technol A* **2015,** *33* (2), 5.
52. Padbury, R. P.; Jur, J. S., Temperature-dependent infiltration of polymers during sequential exposures to trimethylaluminum. *Langmuir* **2014,** *30* (30), 9228-38.

53. Dandley, E. C.; Needham, C. D.; Williams, P. S.; Brozena, A. H.; Oldham, C. J.; Parsons, G. N., Temperature-dependent reaction between trimethylaluminum and poly(methyl methacrylate) during sequential vapor infiltration: experimental and ab initio analysis. *J. Mater. Chem. C* **2014,** *2* (44), 9416-9424.
54. Hill, G. T.; Lee, D. T.; Williams, P. S.; Needham, C. D.; Dandley, E. C.; Oldham, C. J.; Parsons, G. N., Insight on the Sequential Vapor Infiltration Mechanisms of Trimethylaluminum with Poly(methyl methacrylate), Poly(vinylpyrrolidone), and Poly(acrylic acid). *Journal of Physical Chemistry C* **2019,** *123* (26), 16146-16152.
55. Biswas, M.; Libera, J. A.; Darling, S. B.; Elam, J. W., Kinetics for the Sequential Infiltration Synthesis of Alumina in Poly(methyl methacrylate): An Infrared Spectroscopic Study. *Journal of Physical Chemistry C* **2015,** *119* (26), 14585-14592.
56. Biswas, M.; Libera, J. A.; Darling, S. B.; Elam, J. W., New Insight into the Mechanism of Sequential Infiltration Synthesis from Infrared Spectroscopy. *Chem. Mat.* **2014,** *26* (21), 6135-6141.
57. Weisbord, I.; Shomrat, N.; Azoulay, R.; Kaushansky, A.; Segal-Peretz, T., Understanding and Controlling Polymer-Organometallic Precursor Interactions in Sequential Infiltration Synthesis. *Chem. Mat.* **2020,** *32* (11), 4499-4508.
58. Ren, Y.; McGuinness, E. K.; Huang, C.; Joseph, V. R.; Lively, R. P.; Losego, M. D., Reaction–Diffusion Transport Model to Predict Precursor Uptake and Spatial Distribution in Vapor-Phase Infiltration Processes. *Chem. Mat.* **2021,** *33* (13), 5210-5222.
59. Padbury, R. P.; Jur, J. S., Comparison of precursor infiltration into polymer thin films via atomic layer deposition and sequential vapor infiltration using in-situ quartz crystal microgravimetry. *J Vac Sci Technol A* **2014,** *32* (4), 041602-041602.
60. Dwarakanath, S.; Raj, P. M.; Kondekar, N.; Losego, M. D.; Tummala, R., Vapor phase infiltration of aluminum oxide into benzocyclobutene-based polymer dielectrics to increase adhesion strength to thin film metal interconnects. *J Vac Sci Technol A* **2020,** *38* (3), 033210.
61. Dorsey, G. A., The Characterization of Anodic Aluminas. *Journal of The Electrochemical Society* **1966,** *113* (2).
62. Guan, X. H.; Chen, G. H.; Shang, C., ATR-FTIR and XPS study on the structure of complexes formed upon the adsorption of simple organic acids on aluminum hydroxide. *Journal of Environmental Sciences* **2007,** *19* (4), 438-443.
63. Tarte, P., Infra-Red Spectra of Inorganic Aluminates and Characteristic Vibrational Frequencies of Alo4 Tetrahedra and Alo6 Octahedra. *Spectrochimica Acta Part a-Molecular Spectroscopy* **1967,** *A 23* (7), 2127-&.
64. Krishna Priya, G.; Padmaja, P.; Warrier, K. G. K.; Damodaran, A. D.; Aruldhas, G., Dehydroxylation and high temperature phase formation in sol-gel boehmite characterized by Fourier transform infrared spectroscopy. *Journal of Materials Science Letters* **1997,** *16* (19), 1584-1587.
65. Ingram-Jones, V. J.; Slade, R. C. T.; Davies, T. W.; Southern, J. C.; Salvador, S., Dehydroxylation sequences of gibbsite and boehmite: study of differences between soak and flash calcination and of particle-size effects. *J. Mater. Chem.* **1996,** *6* (1).
66. Colomban, P., Raman study of the formation of transition alumina single crystal from protonic ?/?? aluminas. *Journal of Materials Science Letters* **1988,** *7* (12), 1324-1326.
67. Frederickson, L. D., Characterization of Hydrated Aluminas by Infrared Spectroscopy - Application to Study of Bauxite Ores. *Analytical Chemistry* **1954,** *26* (12), 1883-1885.
68. Willis, S. A.; McGuinness, E. K.; Li, Y.; Losego, M. D., Re-examination of the Aqueous Stability of Atomic Layer Deposited (ALD) Amorphous Alumina (Al2O3) Thin Films and the Use of a Postdeposition Air Plasma Anneal to Enhance Stability. *Langmuir* **2021,** *37* (49), 14509-14519.